

A Dusty Mg II absorber Associated with the Quasar SDSS J003545.13+011441.2¹

P. Jiang^{1,2}, J. Ge², J. X. Prochaska^{3,4}, V. P. Kulkarni⁵, H. L. Lu¹, and H. Y. Zhou¹

jpaty@mail.ustc.edu.cn

ABSTRACT

We report on a dusty Mg II absorber associated with the quasar SDSS J003545.13+011441.2 (hereafter J0035+0114) at $z=1.5501$, which is the strongest one among the three Mg II absorbers along the sight line of quasar. The two low redshift intervening absorbers are at $z=0.7436$, 0.5436 , respectively. Based on the photometric and spectroscopic data of Sloan Digital Sky Survey (hereafter SDSS), we infer the rest frame color excess $E(B-V)$ due to the associated dust is more than 0.07 by assuming a Small Magellanic Cloud (hereafter SMC) type extinction curve. Our follow-up moderate resolution spectroscopic observation at the 10-m Keck telescope with the ESI spectrometer enable us to reliably identify most of the important metal elements, such as Zn, Fe, Mn, Mg, Al, Si, Cr, and Ni in the associated system. We measure the column density of each species and detect significant dust depletion. In addition, we develop a simulation technique to gauge the significance of 2175-Å dust absorption bump on the SDSS quasar spectra. By using it, we analyze the SDSS spectrum of J0035+0114 for the presence of a associated 2175-Å extinction feature and report a tentative detection at $\sim 2\sigma$ significant level.

Subject headings: dust, extinction — galaxies: abundances — galaxies: active — quasars: absorption lines — quasars: individual (SDSS J003545.13+0.11441.2)

¹Key Laboratory for Research in Galaxies and Cosmology, The University of Science and Technology of China, Chinese Academy of Sciences, Hefei, Anhui, 230026, China

²Astronomy Department, University of Florida, 211 Bryant Space Science Center, P. O. Box 112055, Gainesville, FL 32611

³University of California Observatories-Lick Observatory, University of California, Santa Cruz, CA 95064

⁴Department of Astronomy and Astrophysics, University of California, Santa Cruz, CA 95064

⁵Department of Physics and Astronomy, University of South Carolina, Columbia, SC 29208

1. Introduction

Absorption lines in the spectra of quasars have been detected since shortly after the discovery of quasars (e.g. Burbidge, Lynds & Burbidge 1966; Schmidt 1966). They provide us with a powerful tool to probe abundances, physical conditions and kinematics of gas in a wide variety of environments. The absorption systems could be divided into two populations by the difference between the redshift of absorption lines (z_{abs}) and the redshift of quasar emission lines (z_{em}). If z_{abs} and z_{em} are almost the same ($z_{abs} - z_{em} < 5,000 \text{ km s}^{-1}$ in quasar rest frame), the absorption system is taken to be associated with the quasar. Otherwise the absorption system is usually intervening (Weymann et al. 1979, Foltz et al. 1986), although some associated C IV absorbers may be found at relative velocities of as much as 75,000 km/s with respect to the quasar (Richards et al. 1999).

The presence of dust grains associated with varieties of absorbers could be constrained by measuring the relative abundances of volatile and refractory elements in order to infer a dust depletion level. The depletion of Cr with respect to Zn in intervening Damped Ly α Absorption systems (DLAs) shows the existence of dust in the high density gas (e.g. Pettini et al. 1994, 1997, 1999; Nestor et al. 2003) All of the DLAs showing high dust depletion level, $[Zn/Fe] > 0.8$, have high molecular hydrogen detection rate (e.g. Ge & Bechtold 1997; Ge et al. 2001; Cui et al. 2005; Noterdaeme et al. 2008).

Dust in an absorber could also be inferred by measuring reddening and extinction effects on the background objects. York et al. (2006) studied the extinction of 809 intervening Mg II absorption systems from the SDSS in a statistical way at $1 \leq z_{abs} < 2$. Their extracted average extinction curves were similar to the SMC curve with $E(B-V) \leq 0.08$, and indicated a tentative correlation between $E(B-V)$ and the Mg II equivalent width in the rest frame $W_0^{\lambda 2796}$. Recently, Ménard et al. (2008) composed a much larger sample with almost 7000 strong Mg II absorption systems at $0.4 < z_{abs} < 2.2$ and confirmed the correlation between $E(B-V)$ and $W_0^{\lambda 2796}$.

The prominent difference between extinction curves of Milky Way (MW) and that of the SMC is the presence of a 2175-Å dust absorption bump (Savage & Mathis 1979; Fitzpatrick 1989). Reliable detections of the 2175-Å feature in individual intervening absorption system are rare. Cohen et al. (1999) detected the 2175-Å feature in a damped Ly α absorber at a redshift of $z=0.524$ toward the BL Lac object AO 0235+164 (later updated by Junkkarinen

¹Some of the data presented herein were obtained at the W.M. Keck Observatory, which is operated as a scientific partnership among the California Institute of Technology, the University of California and the National Aeronautics and Space Administration. The Observatory was made possible by the generous financial support of the W.M. Keck Foundation.

et al. 2004). And Wang et al. (2004) identified three intervening Mg II absorption systems at $1.4 < z < 1.5$ with the 2175-Å dust absorption feature in quasar spectra from the SDSS. Srianand et al. (2008) found a 2175-Å extinction feature in two Mg II systems at $z \sim 1.3$ and detected 21-cm absorption in both of them, which usually traces cold dense gas content. Recently, Noterdaeme et al (2009) presented a detection of carbon monoxide molecules (CO) at $z = 1.6408$ towards a red quasar and a pronounced 2175-Å bump at the redshift of CO absorber. In the past several years, analysis of GRB afterglow spectra has also revealed several positive detections from intervening absorbers and from gas in the GRB host galaxies (e.g. Ellison et al. 2006; Elíasdóttir et al. 2009; Prochaska et al. 2009).

In this paper, we report on a dusty Mg II absorber associated with the quasar SDSS J0035+0114 at $z=1.5501$. In the next section, we will describe the observation data, including SDSS spectrum and our follow-up spectroscopic observation at the 10-m Keck telescope with ESI spectrometer. In §3, we infer the color excess $E(B-V)$ of dust extinction with SDSS photometric and spectroscopic data. In §4, we measure the column densities of important metal ions with high accuracy on Keck spectrum and explore the dust depletion patterns in the absorber. The possible detection of 2175-Å absorption bump will be discussed in §5. Our main results will be summarized in the last section, together with a discussion.

2. Observations

The SDSS images of J0035+0114 were acquired on UT 2001 Oct 15. The point-spread function magnitudes measured from the images are 19.997 ± 0.040 , 19.293 ± 0.010 , 18.972 ± 0.010 , 18.493 ± 0.012 , and 18.344 ± 0.048 in u , g , r , i , and z , respectively. The SDSS spectrum was obtained on UT 2000 Sep 06 and covers $\sim 3800 - 9200$ Å with a spectral resolution $R \sim 2000$ and a median S/N ≈ 7 (Stoughton et al. 2002). The SDSS spectrum is remarkable with relatively red color and strong associated absorption lines imposed on it. Because our initial inspection suggested a very dusty system, we performed follow-up spectroscopic observations of the quasar at higher spectral resolution. On UT 2004 Sep 11, we acquired two 1200s exposures of J0035+0114 with the ESI spectrometer (Sheinis et al. 2002) on the 10m Keck II telescope. We employed the 0.5" slit providing a $\text{FWHM} \approx 37 \text{ km s}^{-1}$ resolution and a wavelength coverage $\lambda = 4000 - 10,000$ Å. The spectral images were reduced and calibrated using the XIDL² software package ESIRedux³ (v1.0). The optimally extracted 1D spectra were converted to vacuum wavelengths and converted to the heliocentric frame and then

²<http://www.ucolick.org/~xavier/IDL>

³<http://www2.keck.hawaii.edu/inst/esi/ESIRedux/index.html>

flux-calibrated using a spectrophotometric standard acquired that same night. The data were normalized by fitting a series of polynomials to absorption-free regions of the quasar spectrum. The emission redshift of $z = 1.5501$ is measured.

3. Color and Reddening

The color of quasars is redshift dependent, since the broad emission features on underlying continuum move in/out the photometric passbands at different redshift (Richards et al. 2001). Richards et al. (2003) introduced a relative color to determine the underlying continuum color of quasars by subtracting the median colors of quasars at the redshift of each quasar from the measured colors of each quasar. The relative color $\Delta(g-i)$ can be used to distinguish between reddened quasars and optically steep quasars. The distribution of relative colors should be a Gaussian, assuming a Gaussian distribution of power-law spectral indices of quasars. However, $\Delta(g-i)$ shows a significant asymmetric tail to the red end. The objects in this tail are reddened by dust.

The relative color $\Delta(g-i)$ of J0035+0114 is 0.40 ± 0.02 . $\Delta(g-i)$ s of all quasars with redshift between 1.525 and 1.575 in SDSS Data Release 7 (Abazajian et al. 2009) are extracted to compose the relative color distribution at the redshift of J0035+0114 ($z=1.5501$). All the colors in this analysis are dereddened by using the dust map of Schlegel et al. (1998). In Figure 1, it is clear that J0035+0114 is in the red tail of the composed color distribution. By assuming the intrinsic spectral index of J0035+0114 is flat ($\Delta(g-i)=0$), we infer that it could be reddened by an SMC type extinction curve with $E(B-V) \sim 0.09$ in the rest frame of quasar emissions at $z=1.5501$ (Richards et al. 2003).

On the Keck spectrum of J0035+0114, three absorption line systems can be readily identified, with redshifts of $z=1.5501$, 0.7436, and 0.5436, respectively (hereafter system-A, -B, and -C). The Mg II $\lambda\lambda 2796, 2803$ doublet has been detected in all of the three systems. The Mg II $\lambda 2796$ absorption line in system-A is the strongest with rest equivalent width $W_0^{\lambda 2796} = 1.986 \pm 0.022$ ($W_0^{\lambda 2796} = 1.622 \pm 0.186$ in system-B; $W_0^{\lambda 2796} = 0.923 \pm 0.182$ in system-C). To examine the dust reddening on SDSS spectrum of J0035+0114, we fit it⁴ with two reddened composite SDSS quasar spectrum models. First, we assume the dust reddening is solely due to system-A, which is the strongest one. The composite SDSS spectrum (Vanden Berk et al. 2001) is reddened by SMC type extinction curve (Pei 1992), in which $E(B-V)$ is a free parameter and $R_V = 2.93$ is fixed, at $z=1.5501$. To focus on fitting continuum of

⁴ The SDSS spectrum has been corrected for the Galactic reddening of $E(B-V)=0.022$ before fitting procedure.

quasar spectrum, the regions with strong emission lines and known strong absorption lines are masked. The best fitted $E(B-V)$ is 0.15, with $\chi^2_\nu=1.28$ (see Figure 2a). Second, we fit the SDSS spectrum with a three absorbers model. We assume the total dust reddening is contributed by three SMC extinction curves with the same $E(B-V)$ at the redshifts of 1.5501, 0.7436, 0.5436. The best fitted $E(B-V)$ is 0.07, with $\chi^2_\nu=1.28$ (see Figure 2b). Since system-A is the strongest absorber, we infer that its rest frame $E(B-V)$ would be greater than 0.07, which is the average reddening of the three absorbers, by assuming $E(B-V)$ scales with $W_0^{\lambda 2796}$ in strong quasar Mg II absorption systems (Ménard et al. 2008).

4. Column Density and Dust Depletion

Most of the important heavy elements are reliably identified in system -A (see Figure 3). Column densities of all elemental ions except Zn^+ were first estimated by measuring the apparent optical depth (AOD, Savage & Sembach 1991). $\text{Zn II } \lambda\lambda 2026, 2062$ are heavily blended with $\text{Mg I } \lambda 2026$ and $\text{Cr II } \lambda 2062$. To measure the column density of zinc, we first fitted $\text{Mg I } \lambda 2852$ with a single Voigt profile, and then fitted $\text{Mg I } \lambda 2026$, $\text{Zn II } \lambda\lambda 2026, 2062$, and $\text{Cr } \lambda\lambda 2056, 2062, 2066$ simultaneously using the modeled profile of $\text{Mg I } \lambda 2852$ as a template for each line. The multi-Voigt fitting gave a column density of $\log N(\text{Zn II})=13.21 \pm 0.03$. In addition, we fitted the Fe II multiplets with Voigt profile fitting of multiple lines. The fitting of Fe II $\lambda\lambda 2249, 2260$ together gave a column density of $\log N(\text{Fe II})=15.2 \pm 0.04$. While the fitting of Fe II $\lambda\lambda 2344, 2374, 2382$ together gave a value of 14.88 ± 0.03 . The equivalent width and column density measured from ionized lines are presented in Table 1. We also measure the column densities of strong Mg II and Fe II absorption lines in system-B and system-C (see Table 2 and Figure 4).

“The expanded SDSS/HST sample of low-redshift DLAs”, compiled by Rao et al. (2006), shows the success rate of DLA detection is $42\% \pm 7\%$ for strong Mg II–Fe II systems with $W_0^{\lambda 2796}/W_0^{\lambda 2600} < 2$ and $\text{Mg I } W_0^{\lambda 2852} \gtrsim 0.1 \text{ \AA}$. The associated Mg II absorber here is right in this high detection rate region and it may therefore be a dusty DLA absorption system. However, it is at low redshift $z < 1.65$, where the $\text{Ly}\alpha$ transition cannot be observed in optical band with ground instruments. Thus, the column density of neutral hydrogen $N(\text{H I})$ cannot be measured. Since there are no lines of high ions detected in the Keck spectrum (except for Al III), we assume that hydrogen gas is mostly neutral and other heavy elements are singly ionized in this Mg II absorption system while measuring column densities and dust depletion levels.

The presence of dust grains could be constrained by measuring the relative abundances of volatile and refractory elements in order to infer a depletion level of metal in

gas phase. As zinc is a relatively undepleted element due to its low condensation temperature, the ratios of other heavy elements to it are usually used to measure the dust depletion (Meyer & Roth 1990; Pettini et al. 1994). The depletion factors, $[X/Zn]=\log(N(X)/N(Zn))-\log(N(X)/N(Zn))_{\odot}$, are listed in Table 3. It is clear that the absorber associated with J0035+0114 has significant depletion factors⁵, which indicates that this system contains substantial dust grains. Figure 5 plots the dust depletion patterns compared with the “warm” and “cold” Galactic interstellar medium (ISM) and SMC ISM. It seems that the depletion pattern in this absorber is similar to those found in sight lines through “warm” gas of MW.

5. Possible 2175-Å Absorption Bump

Initially the quasar absorption line system in J0035+0114 at $z=1.5501$ is a candidate in our ongoing project to search for quasar absorption line systems with 2175-Å absorption bump feature (Zhou et al. 2010). It was selected because the suppressed flux of quasar around 2200-Å in the rest frame of the associated Mg II absorber. However, the depression can be caused by the variation of the strength of Fe II emissions, too (Pitman et al. 2000). Hence, we develop a simulation technique to gauge the significance of 2175-Å dust absorption bump on the SDSS quasar spectra.

J0035+0114 is taken as an example to introduce our simulation procedures below. First, all the SDSS spectra of quasar with emission redshift in the range of $z_{J0035}-0.05$ and $z_{J0035}+0.05$ with median $S/N > 6$ are chosen to compose a control sample and then are corrected for Galactic reddening. We basically fit each of them by reddening the composite quasar spectrum (Vanden Berk et al. 2001) with a parameterized extinction curve at redshift of the absorber of interest. The extinction curve is defined in a similar formula with the prescription of Fitzpatrick & Massa (1990), as

$$A(\lambda) = c_1 + c_2x + c_3D(x, x_0, \gamma) \quad (1)$$

where $x = \lambda^{-1}$. And $D(x, x_0, \gamma)$ is a Lorentzian profile, which is expressed as

$$D(x, x_0, \gamma) = \frac{x^2}{(x^2 - x_0^2)^2 + x^2\gamma^2} \quad (2)$$

where x_0 and γ is the peak position and FWHM of Lorentzian profile, respectively. Our aim is to unveil the 2175-Å absorption feature associated with absorption line systems on quasar

⁵Zn II $\lambda\lambda$ 2026,2062 of system-B and system-C are not covered by the Keck spectrum. Thus, the dust depletion patterns in those systems are not obtainable.

spectra. We do not try to derive the absolute extinction curve and our derived one is a relative extinction curve without normalization. We cannot measure the conventional extinction parameters A_V , $E(B-V)$ and R_V from it. But all the features of 2175-Å absorption bump are preserved. The linear component in the extinction curve accounts for the variation of quasar spectral index. Thus, the parameter c_2 could be negative if a quasar spectrum is steeper than composite spectrum. The Lorentzian profile is used to model absorption bump. The strength of bump is measured by the area of bump $A_{bump} = \pi c_3 / (2\gamma)$.⁶ However, this strength is not necessarily zero even if the spectrum does not have any absorption bump feature. In the absence of a bump, the distribution of the best fitted strength is expected to be Gaussian by assuming random fluctuation of Fe II emission on each spectrum and photon noise. During the fitting procedure, x_0 is fixed to $4.59 \mu m^{-1}$ in the rest frame of the absorber of interest and the width γ is fixed to $0.89 \mu m^{-1}$ in the same frame.⁷ The three free parameters are c_1 , c_2 and c_3 . To focus on fitting continuum of quasar spectrum, the regions with strong emission lines (Mg II λ 2800, C III] λ 1909, C IV λ 1550, Si IV λ 1400) and known strong absorption lines are masked.

The SDSS spectrum of J0035+0114 is modeled by a composite quasar spectrum reddened using the parameterized extinction curve at the same redshift of it. Although J0035+0114 could be reddened by three dusty absorbers simultaneously, the two low redshift absorbers (system-B and -C) cannot contribute to the possible 2175-Å extinction bump. In addition, we think the reddening effects of them can be well modeled by the linear component of the parameterized extinction curve. The fitting results are presented in Figure 6: panel (a) shows the best model compared with observation data; panel (b) shows the best fitting extinction curve in the quasar rest frame. The goodness of fit is measured by $\chi^2_\nu = 1.21$. Then, 4576 quasar SDSS spectra around the redshift of J0035+0114 ($z=1.5501$) are selected to compose a fairly big control sample. The histogram of fitted strength of bumps is plotted in Figure 7. It can be fitted by using a single Gaussian function with the standard deviation $\sigma = 0.08$. The strength of bumps extracted on the spectrum of J0035+0114 is 0.15 ± 0.02 . In sense of statistics, the possibility that this bump is a real absorption feature is $\sim 95\%$ (significant at $\sim 2\sigma$ level). Therefore, the 2175-Å absorption bump associated with J0035+0114 is only a marginal detection. In contrast, we measure six significant 2175-Å extinction bumps detected on SDSS spectra in literatures with the same formalism and find that they are at least

⁶The area of bump defined in this work is different from that in Fitzpatrick & Massa (2007). $A_{bump} = E(B-V) \times A_{bump}^*$, where A_{bump}^* is the area defined in FM07. A_{bump} can be interpreted as rescaling the integrated apparent optical depth of bump absorption ($A_\lambda = \frac{2.5}{\ln 10} \tau_\lambda$).

⁷The most likely values of peak and width for Galaxy 2175-Å absorption bump are $4.59 \mu m^{-1}$ and $0.89 \mu m^{-1}$ (Fitzpatrick and Massa, 2007).

five times stronger than the one in this work (see Table 4). The wavelength coverage of SDSS spectrum is from 3800 Å to 9200 Å. It allows us to detect MW-like 2175-Å extinction feature up to redshift $z \sim 3$. The highest redshift for identified 2175-Å bump to date is $z = 3.03$, which was detected by Prochaska et al. (2009) using the afterglow Optical/IR photometry of gamma-ray burst GRB 080607. Another high redshift 2175-Å bump was detected by Elíasdóttir et al. (2009) on the afterglow spectrum of GRB 070802 at $z = 2.45$.

6. Discussion and Summary

The strongest Mg II absorption system presented in this work is probably associated with quasar, since it has $(z_{em} - z_{abs}) \sim 30 \text{ km s}^{-1}$ in quasar rest frame. It is very possible that the corresponding cold gas rises from the host galaxy of quasar. However, we cannot rule out a nearby foreground galaxy absorption scenario.

Interstellar dust grains play an important role in the evolution of galaxies, star formation and planet formation. The dust content in physical environment of quasar has not been well studied (Li 2007 and reference therein). More detection of associated dusty absorption system will aid us to understand the nature of this dust and provide more clues on the evolution of galaxies and quasars. Furthermore, the population of dust-reddened quasars is a possible contributor to the X-ray background (e.g. Shanks et al. 1991; Mushotzky et al. 2000; Brandt et al. 2000; Dong et al. 2005). Its contribution is independent of the contribution of type 2 quasars with completely obscured broad emission line regions (Antonucci 1993).

On the basis of Keck spectroscopic observations, the dust depletion factor, $[\text{Fe}/\text{Zn}] \sim 0.86$, represents the high depletion population in high-redshift DLAs reported in Noterdaeme et al. (2008). All of the previous DLAs showing high dust depletion factor, $[\text{Fe}/\text{Zn}] < 0.8$, have high molecular hydrogen abundance. Thus, this system is very likely associated with high molecular hydrogen content. Unfortunately, the molecular hydrogen absorption bands associated with this system are in the UV region beyond the atmospheric transmission window.

Figure 8 plots the histogram of strength of 2175-Å absorption bump measured on 328 Galactic extinction curves (Fitzpatrick & Massa 2007). The dash lines on left is the 3σ threshold and the one on right is the 5σ threshold suggested by our simulation. If we only accept the detection at confidence level $\geq 5\sigma$, more than 94% of Galactic bumps can be recovered with our approach. The success rate is so promising that we can develop a sensitive method for detecting MW-like 2175-Å extinction bumps on quasar spectra with

Mg II absorption lines in SDSS database (Jiang et al. in preparation). The strength of bumps measured in SMC (Gordon et al. 2003) are also plotted in Figure 8. The extinction curve measured in the sight line of SMC wing exhibits a significant 2175-Å absorption bump.

In summary, we identify three Mg II absorption line systems along the sight line of the quasar J0035+0114. The strongest one is most likely associated with the quasar. The dust content in this associated system is firmly detected by either reddening or elements dust depletion pattern. The extinction curve of this system is more likely to be SMC type with $E(B-V) > 0.07$. However, we detect a tentative 2175-Å extinction bump at $\sim 2\sigma$ significant level with our parameterized extinction curve technique. The high dust content suggest this system is likely a DLA with molecular hydrogen content.

This work was partially supported by NSF with grant NSF AST-0451407, AST-0451408 & AST-0705139 and the University of Florida. PJ acknowledges support from China Scholarship Council. This research has also been partially supported by the CAS/SAFEA International Partnership Program for Creative Research Teams. VPK acknowledges support from NSF grant AST-0607739 to the University of South Carolina.

The authors wish to recognize and acknowledge the very significant cultural role and reverence that the summit of Mauna Kea has always had within the indigenous Hawaiian community. We are most fortunate to have the opportunity to conduct observations from this mountain.

Funding for the SDSS and SDSS-II has been provided by the Alfred P. Sloan Foundation, the Participating Institutions, the National Science Foundation, the U.S. Department of Energy, the National Aeronautics and Space Administration, the Japanese Monbukagakusho, the Max Planck Society, and the Higher Education Funding Council for England. The SDSS Web Site is <http://www.sdss.org/>.

The SDSS is managed by the Astrophysical Research Consortium for the Participating Institutions. The Participating Institutions are the American Museum of Natural History, Astrophysical Institute Potsdam, University of Basel, University of Cambridge, Case Western Reserve University, University of Chicago, Drexel University, Fermilab, the Institute for Advanced Study, the Japan Participation Group, Johns Hopkins University, the Joint Institute for Nuclear Astrophysics, the Kavli Institute for Particle Astrophysics and Cosmology, the Korean Scientist Group, the Chinese Academy of Sciences (LAMOST), Los Alamos National Laboratory, the Max-Planck-Institute for Astronomy (MPIA), the Max-Planck-Institute for Astrophysics (MPA), New Mexico State University, Ohio State University, University of Pittsburgh, University of Portsmouth, Princeton University, the United States Naval Observatory, and the University of Washington.

REFERENCES

- Abazajian, K. N., & for the SDSS Collaboration 2009, *ApJS*, 182, 543
- Antonucci, R. 1993, *ARA&A*, 31, 473
- Asplund, M., Grevesse, N., and Sauval, A. J. 2005, *ASPC*, 336, 25
- Bouchet, P., Lequeux, J., Maurice, E., Prevot, L., and Prevot-Burnichon, M. L. 1985, *A&A*, 149, 330
- Brandt, W. N., et al. 2000, *AJ*, 119, 2349
- Burbidge, E. M., Lynds, C. R., and Burbidge, G. R. 1966, *ApJ*, 144, 447
- Cohen, R. D., Burbidge, E. M., Junkkarinen, V. T., Lyons, R. W., and Madejski, G. 1999, *BAAS*, 31, 942
- Cui, J., Bechtold, J., Ge, J., & Meyer, D.M. 2005, *ApJ*, 633, 649
- Dong, X. B., Zhou, H. Y., Wang, T. G., Wang, J. X., Li, C. and Zhou, Y. Y. 2005, *ApJ*, 620, 629
- Elíasdóttir, Á., Fynbo, J. P. U., Hjorth, J., Ledoux, C., Watson, D. J., Andersen, A. C., Malesani, D., Vreeswijk, P. M., Prochaska, J. X., Sollerman, J., and Jaunsen, A. O. 2009, *ApJ*, 697, 1725
- Ellison, S. L., Vreeswijk, P., Ledoux, C., Willis, J. P., Jaunsen, A., Wijers, R. A. M. J., Smette, A., Fynbo, J. P. U., Møller, P., Hjorth, J., and Kaufer, A. 2006, *MNRAS*, 372, 38
- Fitzpatrick, E. L. 1989, *IAUS*, 135, 37
- Fitzpatrick, E. L., & Massa, D. 1990, *ApJS*, 72, 163
- Fitzpatrick, E. L., & Massa, D. 2007, *ApJ*, 663, 320
- Foltz, C. B., Weymann, R. J., Peterson, B, M., Sun, L., Malkan, M. A., and Chaffee, F. H. 1986, *ApJ*, 307, 504
- Ge, J. Bechtold, J., & Kulkarni, V.P. 2001, *ApJ*, 547, L1
- Ge, J., & Bechtold, J., 1997, *ApJ*, 477, L73
- Gordon, K. D., Clayton, G. C., Misselt, K. A., Landolt, A. U., and Wolff, M. J. 2003, *ApJ*, 594, 279
- Jenkins, E. B., Savage, B. D., and Spitzer, L. 1986, *ApJ*, 301, 355
- Jiang, P., Ge, J., Prochaska, J. X., Wang, J., Zhou, H. Y., and Wang, T. G. 2010, *ApJ*, submitted

- Jiang, P., Ge, J., Zhou, H. Y., Wang, T. G., and Wang, J. X. 2010, in preparation
- Junkkarinen, V. T., Cohen, R. D., Beaver, E. A., Burbidge, E. M., Lyons, R. W., and Madejski, G. 2004, *ApJ*, 614, 658
- Li, A. 2007, *ASPC*, 373, 561
- Ménard, B., Nestor, D. B., Turnshek, D. A., Quider, A. M., Richards, G. T., Chelouche, D., and Rao, S. M. 2008, *MNRAS*, 385, 1053
- Meyer, D. M., and Roth, K. C. 1990, *ApJ*, 363, 57
- Mushotzky, R. F., Cowie, L. L., Barger, A. J., and Arnaud, K. A. 2000, *Nature*, 404, 459
- Nestor, D. B., Rao, S. M., Turnshek, D. A., and vanden Berk, D. 2003, *ApJ*, 595, 5
- Noterdaeme, P., Ledoux, C., Petitjean, P., & Srianand, R. 2008, *A&A*, 481, 327
- Noterdaeme, P., Ledoux, C., Srianand, R., Petitjean, P., and Lopez, S. 2009, *A&A*, 503, 765
- Pei, Y. C. 1992, *ApJ*, 395, 130
- Pettini, M., Smith, L. J., Hunstead, R. W., and King, D. L. 1994, *ApJ*, 426, 79
- Pettini, M., Smith, L. J., King, D. L., and Hunstead, R. W. 1997, *ApJ*, 486, 665
- Pettini, M., Ellison, S. L., Steidel, C. C., and Bowen, D. V. 1999, *ApJ*, 510, 576
- Pitman, K. M., Clayton, G. C., and Gordon, K. D. 2000, *PASP*, 112, 537
- Prochaska, J. X., Sheffer, Y., Perley, D. A., Bloom, J. S., Lopez, L. A., Dessauges-Zavadsky, M., Chen, H.-W., Filippenko, A. V., Ganeshalingam, M., Li, W., Miller, A. A., and Starr, D. 2009, *ApJ*, 691, 27
- Rao, S. M., Turnshek, D. A., and Nestor, D. B. 2006, *ApJ*, 636, 610
- Richards, G. T., York, D. G., Yanny, B., Kollgaard, R. I., Laurent-Muehleisen, S. A., and vanden Berk, D. E. 1999, *ApJ*, 513, 576
- Richards, G. T. et al. 2001, *AJ*, 121, 2308
- Richards, G. T. et al. 2003, *AJ*, 126, 1131
- Savage, B. D., & Mathis, J. S. 1979, *ARA&A*, 17, 73
- Savage, B. D., & Sembach, K. R. 1991, *ApJ*, 379, 245
- Schlegel, D. J., Finkbeiner, D. P., and Davis, M. 1998, *ApJ*, 500, 525
- Schmidt, M. 1966, *ApJ*, 144, 443
- Shanks, T., Georgantopoulos, I., Stewart, G. C., Pounds, K. A., Boyle, B. J., and Griffiths, R. E. 1991, *Nature*, 353, 315

- Sheinis, A. I., Bolte, M., Epps, H. W., Kibrick, R. I., Miller, J. S., Radovan, M. V., Bigelow, B. C., and Sutin, B. M. 2002, *PASP*, 114, 851
- Srianand, R., Gupta, N., Petitjean, P., Noterdaeme, P., and Saikia, D. J. 2008, *MNRAS*, 391, 69
- Stoughton, C. et al. 2002, *SPIE*, 4836, 339
- Vanden Berk, D. E. et al. 2001, *AJ*, 122, 549
- Wang, J., Hall, P. B., Ge, J., Li, A., and Schenider, D. P. 2004, *ApJ*, 609, 589
- Welty, D. E., Hobbs, L. M., Lauroesch, J. T., Morton, D. C., Spitzer, L., and York, D. G. 1999, *ApJS*, 124, 465
- Welty, D. E., Lauroesch, J. T., Blades, J. C., Hobbs, L. M., and York, D. G. 2001, *ApJ*, 554, 75
- Weymann, R. J., Williams, R. E., Peterson, B. M., and Turnshek, D. A. 1979, *ApJ*, 234, 33
- York, D. G. et al. 2006, *MNRAS*, 367, 945
- Zhou, H. Y., Ge, J., Lu, H. L., Wang, T. G., Yuan, W. M., Jiang, P., and Shan, H. G. 2010, *ApJ*, 708, 742

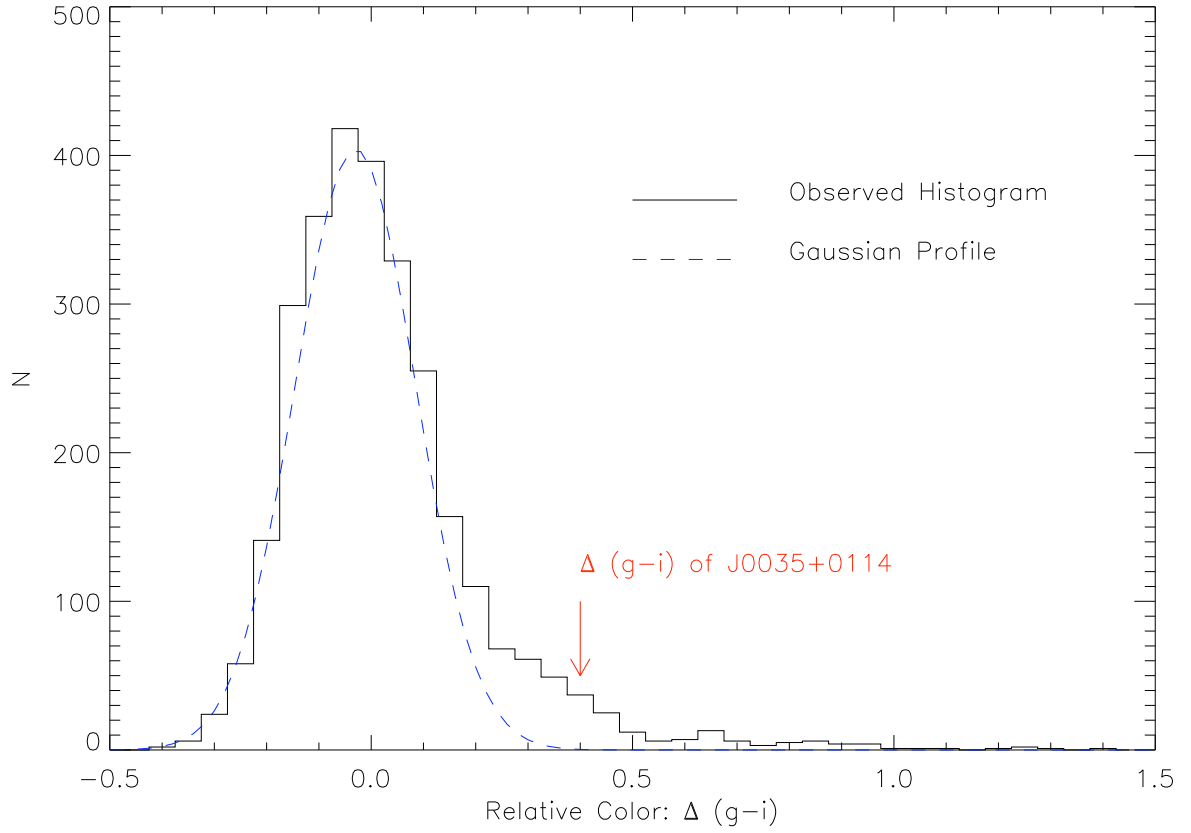


Fig. 1.— The histogram of the relative color $\Delta(g-i)$ of SDSS quasar at redshift range between 1.525 and 1.575. Dashed blue line is a Gaussian fitting the blue wing. The red arrow indicates the relative color of J0035+0114.

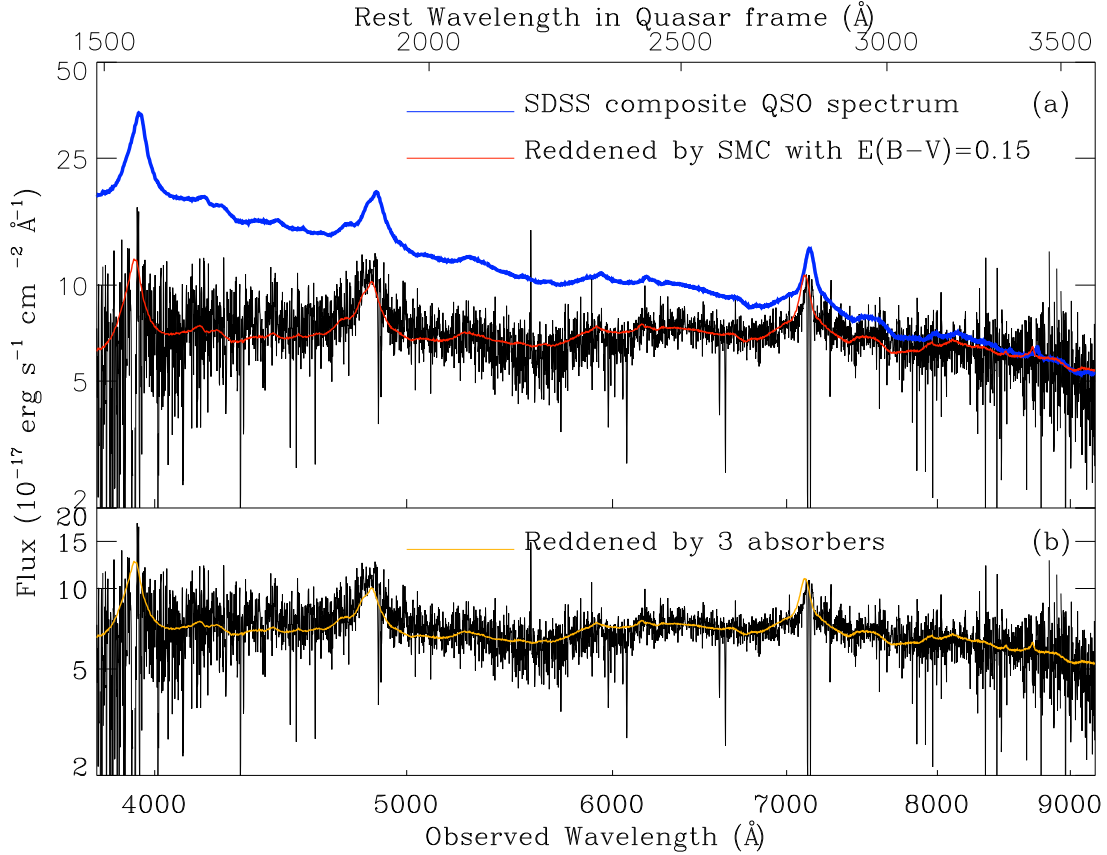


Fig. 2.— In panel (a), the reddened composite quasar spectrum by using SMC extinction curve with $E(B-V)=0.15$ at $z=1.5501$ (the red line) overplotted with SDSS spectrum and the rescaled SDSS composite quasar spectrum (the blue line). The composite spectrum is scaled to match the observed data around 9000 \AA . In panel (b), the three absorbers model, composite spectrum is reddened by three SMC extinction curves with $E(B-V)=0.07$ at $z=1.5501, 0.7436, 0.5436$ (the orange line).

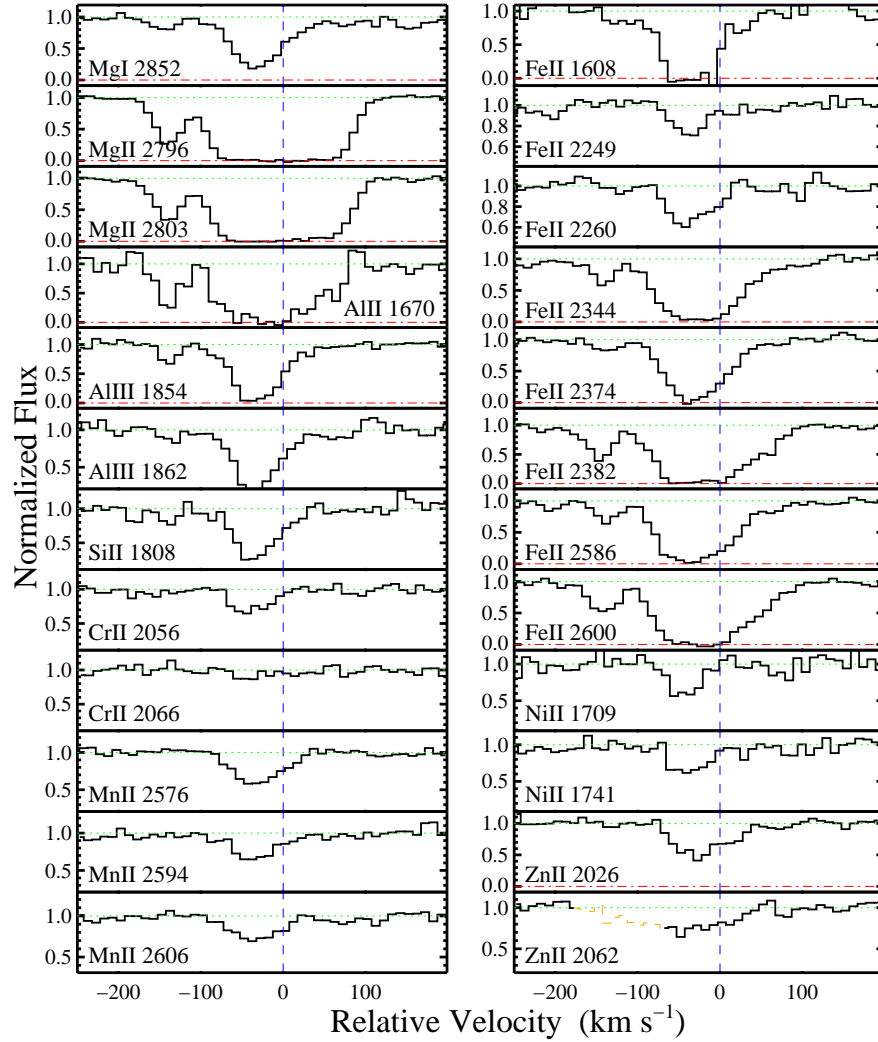


Fig. 3.— Normalized Spectrum of J0035+0114 taken at the 10-m Keck telescope with ESI spectrometer. Strong absorption lines of ionized Fe, Ni, Si, Al, Cr, Mn, Mg, Zn in the associated absorber are plotted in velocity space. The dash lines indicate the $v = 0 \text{ km s}^{-1}$ at redshift 1.5501.

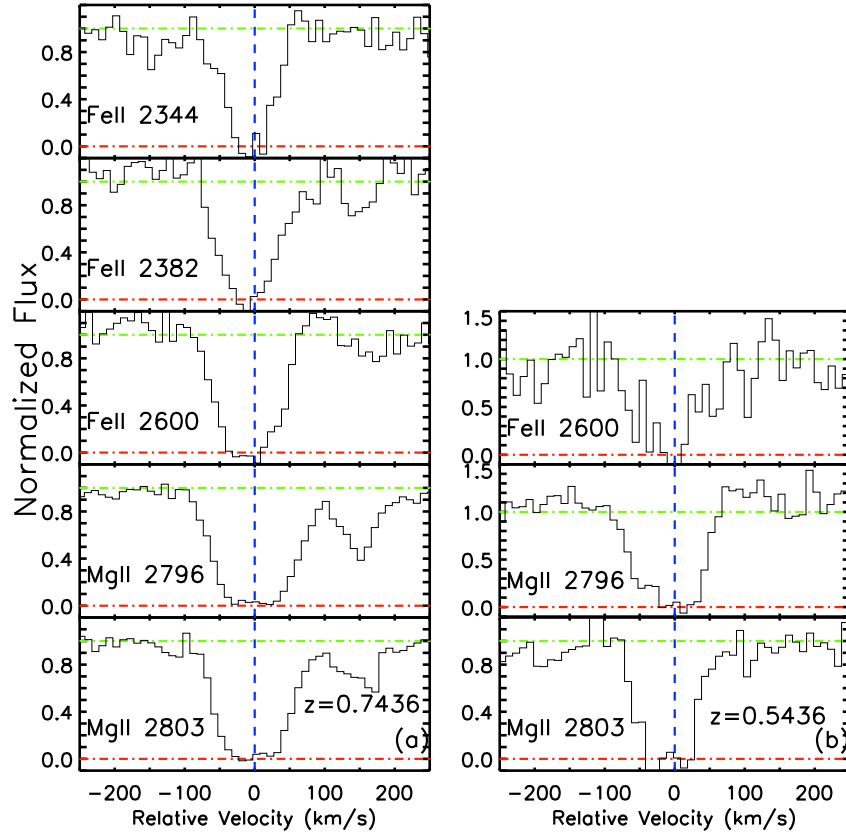


Fig. 4.— Normalized Spectrum of J0035+0114 taken at the 10-m Keck telescope with ESI spectrometer. Panel (a) is the strong absorption lines detected in the intervening absorber at $z=0.7436$; Panel (b) is the strong absorption lines detected in the intervening absorber at $z=0.5436$. The dash lines indicate the $v = 0 \text{ km s}^{-1}$ in the rest frame of interested absorber.

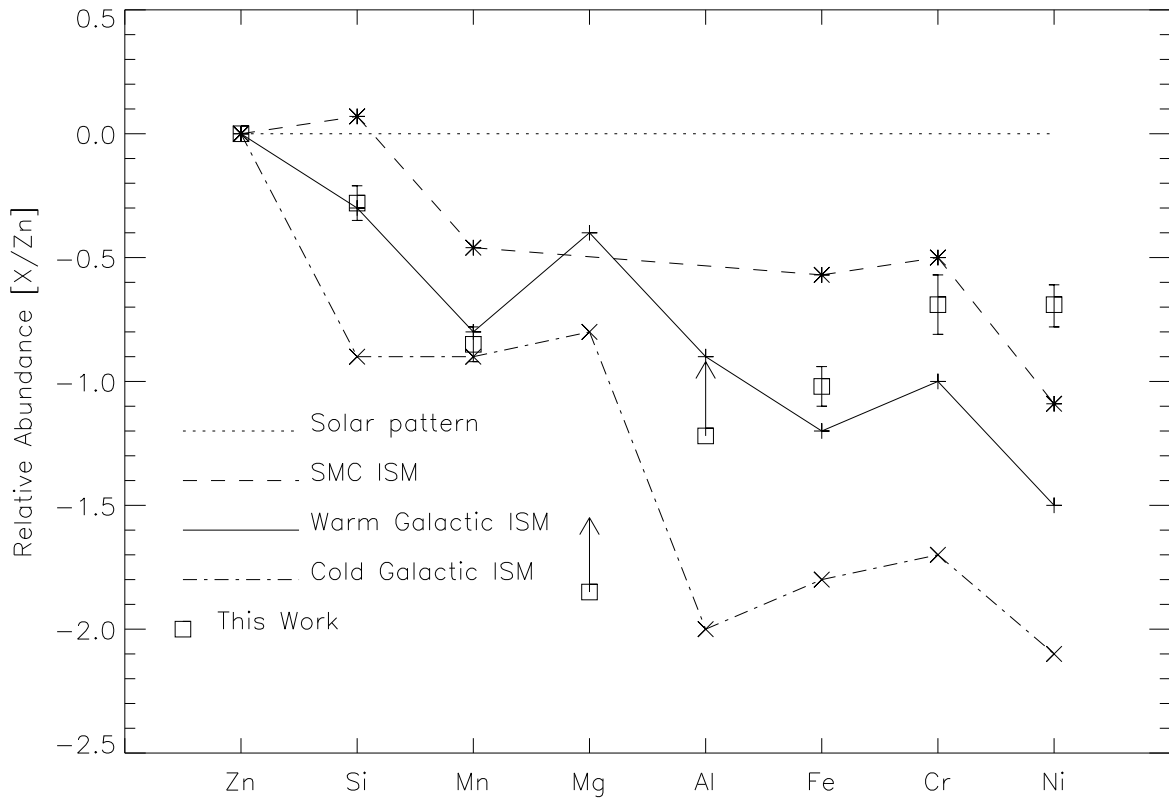


Fig. 5.— Relative abundances are measured in J0035+0114 and compared with other known dusty clouds. Values for “warm” and “cold” Galactic ISM and SMC ISM were adopted from Jenkins et al. 1986, Welty et al. 1999 and Welty et al. 2001.

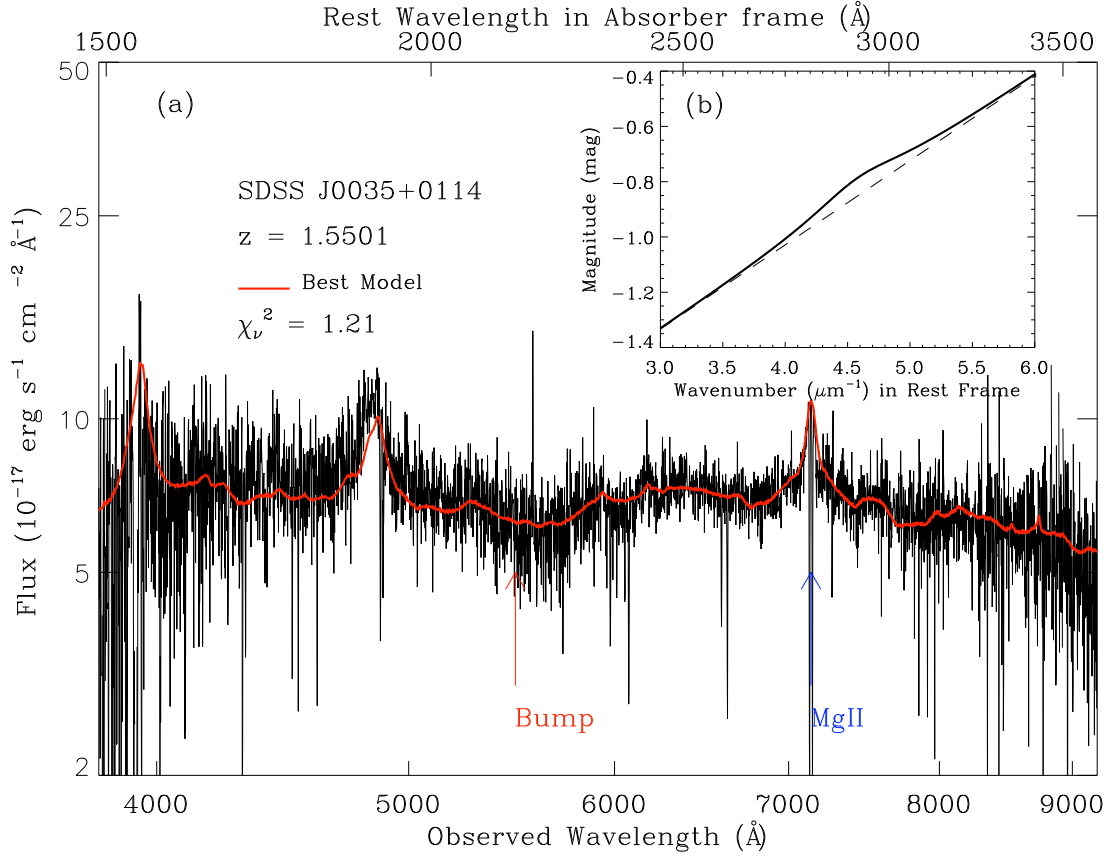


Fig. 6.— In panel (a), the best fitted model is plotted with the observed data in the frame of observer. The red arrow indicates the center of fitted 2175-Å absorption bump and the blue arrow indicates the Mg II absorption lines. In panel (b), the solid line is the best fitted extinction curve in rest frame of absorber. Its linear component is plotted with dashed line.

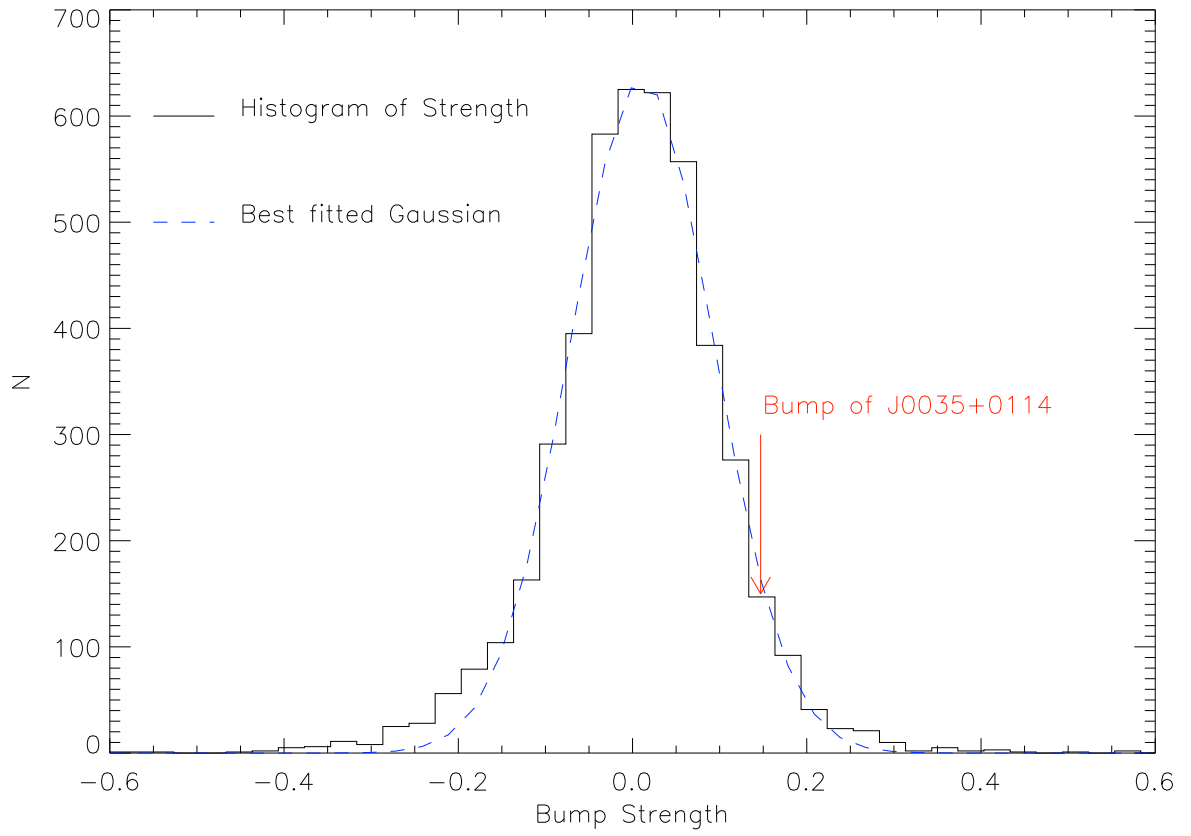


Fig. 7.— The histogram of strength of bumps extracted in the simulation is presented in black line. The dashed blue line is the best fitted Gaussian. The red arrow indicates the strength of bump in J0035+0114.

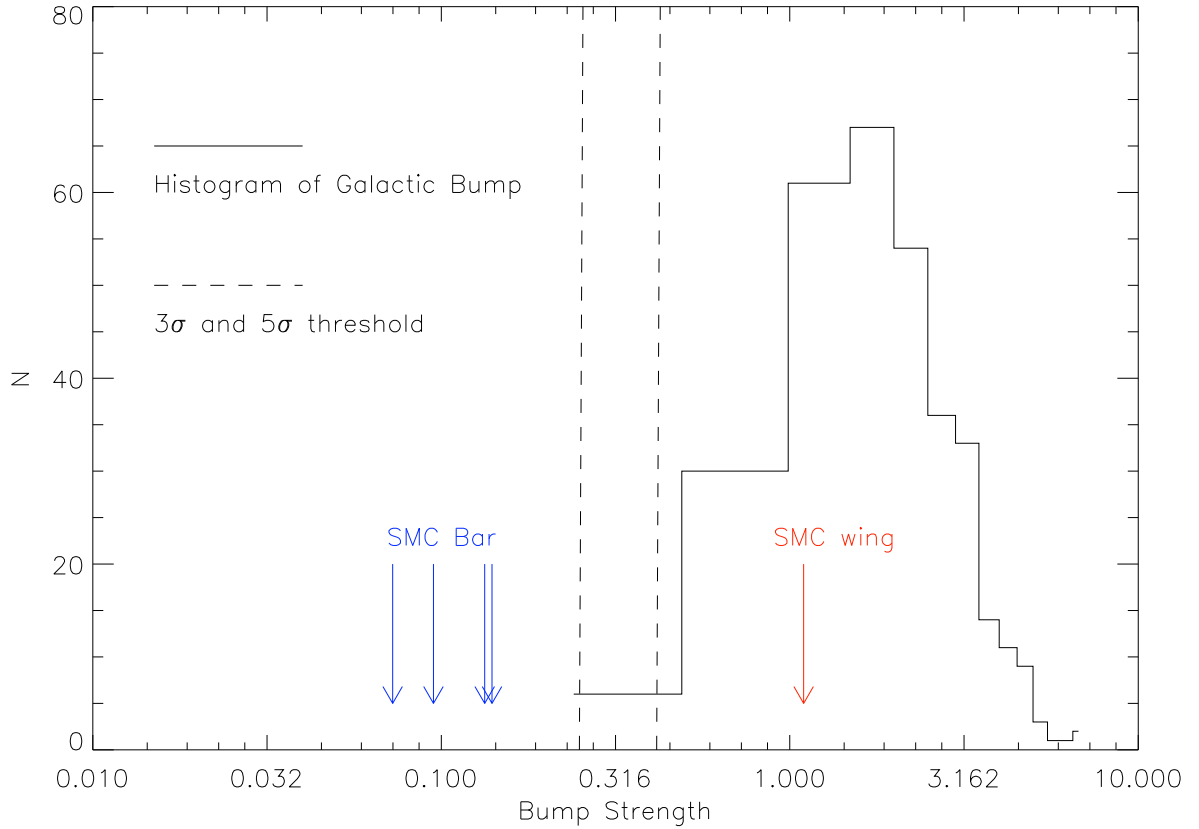


Fig. 8.— The histogram of strength of 2175-Å absorption bumps measured on 328 Galactic extinction curves (Fitzpatrick & Massa 2007). The dash lines are the 3σ and 5σ thresholds suggested by the simulation. Blue arrows indicate the bump strength measured in sight lines of SMC bar and the red arrow indicated the bump strength measured in sight line of SMC wing (Gordon et al 2003).

Table 1. Associated Strong Absorption Lines and Column Density measured by Apparent Optical Depth

λ_{vacuum} (Å)	Ion	f	λ^a (Å)	EW ^a (Å)	N_X^b log(cm ⁻²)	N_X^c log(cm ⁻²)
1608.4511	Fe II	0.0580	1608.437	0.516±0.043	14.98 ^{+0.02} _{-0.02}	...
1670.7874	Al II	1.8800	1670.822	0.883±0.046	13.71 ^{+0.02} _{-0.01}	...
1709.6042	Ni II	0.0324	1709.558	0.103±0.022	14.18 ^{+0.06} _{-0.07}	...
1741.5531	Ni II	0.0427	1741.591	0.124±0.022	14.11 ^{+0.05} _{-0.07}	...
1808.0130	Si II	0.0022	1808.035	0.278±0.026	15.84 ^{+0.03} _{-0.03}	...
1854.7164	Al III	0.5390	1854.704	0.520±0.035	13.80 ^{+0.02} _{-0.01}	...
1862.7895	Al III	0.2680	1862.805	0.401±0.036	13.86 ^{+0.03} _{-0.03}	...
2026.136	Zn II	0.4890	2026.277 ^d	0.286±0.022	13.30 ^{+0.03} _{-0.03}	13.21 ^{+0.03} _{-0.03}
2026.4768	Mg I	0.1120	2026.277 ^e	0.286±0.022	13.95 ^{+0.03} _{-0.03}	...
2056.2539	Cr II	0.1050	2056.236	0.123±0.017	13.57 ^{+0.04} _{-0.05}	...
2062.234	Cr II	0.0780	2062.563 ^f	0.242±0.029	13.98 ^{+0.04} _{-0.05}	...
2062.664	Zn II	0.2560	2062.556 ^g	0.224±0.031	13.47 ^{+0.05} _{-0.05}	13.21 ^{+0.03} _{-0.03}
2066.1610	Cr II	0.0515	2066.282	0.053±0.022	13.46 ^{+0.13} _{-0.18}	...
2249.8768	Fe II	0.0018	2249.905	0.106±0.025	15.17 ^{+0.07} _{-0.09}	15.20 ^{+0.04} _{-0.04}
2260.7805	Fe II	0.0024	2260.781	0.154±0.022	15.22 ^{+0.04} _{-0.05}	15.20 ^{+0.04} _{-0.04}
2344.2140	Fe II	0.1140	2344.265	1.003±0.043	14.62 ^{+0.01} _{-0.01}	14.88 ^{+0.03} _{-0.03}
2374.4612	Fe II	0.0313	2374.482	0.731±0.031	15.00 ^{+0.01} _{-0.01}	14.88 ^{+0.03} _{-0.03}
2382.7650	Fe II	0.3200	2382.779	1.295±0.034	14.33 ^{+0.01} _{-0.01}	14.88 ^{+0.03} _{-0.03}
2576.8770	Mn II	0.3508	2576.927	0.240±0.023	13.14 ^{+0.03} _{-0.04}	...
2586.6500	Fe II	0.0691	2586.659	0.977±0.034	14.73 ^{+0.01} _{-0.01}	...
2594.4990	Mn II	0.2710	2594.506	0.176±0.022	13.09 ^{+0.04} _{-0.05}	...
2600.1729	Fe II	0.2390	2600.233	1.328±0.031	14.42 ^{+0.01} _{-0.01}	...
2606.4620	Mn II	0.1927	2606.470	0.168±0.020	13.20 ^{+0.04} _{-0.04}	...
2796.3520	Mg II	0.6123	2796.563	1.986±0.022	14.22 ^{+0.01} _{-0.01}	...
2803.5310	Mg II	0.3054	2803.964	1.896±0.022	14.49 ^{+0.01} _{-0.01}	...
2852.9642	Mg I	1.8100	2853.018	0.534±0.022	12.81 ^{+0.01} _{-0.01}	...

Note. — Equivalent width is measured in the absorber rest frame at the redshift of 1.5501. Vacuum wavelengths and oscillator strength f are adopted from the Atomic Data conducted by J. X. Prochaska (<http://kingpin.ucsd.edu/~hiresdla/atomic.dat>). All statistical uncertainties reported are 1σ confidence. However, the systematic error of column densities can exceed 0.05 dex due to continuum fitting and line saturation with ESI data.

^aCentral wavelengths and equivalent widths are reported in the absorber rest frame.

^bColumn densities are measured by the Apparent Optical Depth (AOD).

^cColumn densities are measured by multi-Voigt fitting.

^dWe assume blend lines at 2026-Å were all Zn II 2026 when integrating AOD.

^eWe assume blend lines at 2026-Å were all Mg I 2026 when integrating AOD.

^fWe assume blend lines at 2062-Å were all Cr II 2062 when integrating AOD.

^gWe assume blend lines at 2062-Å were all Zn II 2062 when integrating AOD.

Table 2. Intervening Strong Absorption Lines and Column Density measured by Apparent Optical Depth

λ_{vacuum} (Å)	Ion	Redshift	EW (Å)	N_X $\log(\text{cm}^{-2})$
2344.2140	Fe II	0.7436	0.652±0.200	14.48 ^{+0.06} _{-0.06}
2382.7650	Fe II		0.829±0.210	14.12 ^{+0.06} _{-0.06}
2600.1729	Fe II		0.920±0.211	14.32 ^{+0.08} _{-0.08}
2796.3520	Mg II	0.5436	1.622±0.186	14.06 ^{+0.04} _{-0.04}
2803.5310	Mg II		1.408±0.207	14.03 ^{+0.04} _{-0.04}
2600.1729	Fe II		0.879±0.418	14.13 ^{+0.21} _{-0.21}
2796.3520	Mg II	0.976±0.155	0.923±0.182	13.81 ^{+0.30} _{-0.30}
2803.5310	Mg II		0.976±0.155	14.15 ^{+0.20} _{-0.20}

Note. — Equivalent width is measured in the rest frame of interested absorber. See note of Table 1 for the oscillator strengths and systematic errors.

Table 3. Relative Abundances and Dust Depletions in Associated Absorber

Element	N_{adopted} $\log(\text{cm}^{-2})$	$[X/Zn]$	$[X/Zn]_{SMC}^a$	$[X/Zn]_{MKW}^a$	$[X/Zn]_{MKC}^a$
Mg.....	>14.36	>-1.78	...	-0.4	-0.8
Al ^b	>13.83	>-1.15	...	-0.9	-2.0
Si.....	$15.84_{-0.06}^{+0.06}$	$-0.28_{-0.07}^{+0.07}$	0.07	-0.3	-0.9
Cr.....	$13.56_{-0.06}^{+0.06}$	$-0.69_{-0.11}^{+0.11}$	-0.50	-1.0	-1.7
Mn.....	$13.15_{-0.06}^{+0.05}$	$-0.85_{-0.06}^{+0.06}$	-0.46	-0.8	-0.9
Fe.....	$15.20_{-0.06}^{+0.06}$	$-0.86_{-0.08}^{+0.08}$	-0.57	-1.2	-1.8
Ni.....	$14.15_{-0.08}^{+0.08}$	$-0.69_{-0.09}^{+0.09}$	-1.09	-1.5	-2.1
Zn.....	$13.21_{-0.06}^{+0.06}$	0.00	0.00	0.0	0.0

Note. — The solar photospheric values are adopted from Asplund et al. (2005). For the species with several absorption lines detected, the weighted mean column density of unsaturated lines is used to calculate depletion. The column density measured by multi-Voigt fitting is used when it is available. Errors in column densities are combined quadratically while calculating $[X/Zn]$.

^aDust depletion in “warm” and “cold” Galactic ISM (MKW and MKC) and SMC ISM were adopted from Jenkins et al. 1986, Welty et al. 1999 and Welty et al. 2001

^bNo ionization correction was applied, we just use the column density of Al⁺ here.

Table 4. Parameters of Optical/UV Extinction Curves

Reddened Object	z_{abs}^a	c_1 (mag)	c_2 (mag)	c_3 (mag)	x_0 (μm^{-1})	γ (μm^{-1})	Λ_{bump}	χ^2_ν	Reference
J003545.13+011441.2	1.5501	-2.17±0.01	0.28±0.01	0.08±0.01	4.59 ^b	0.89 ^b	0.15±0.02	1.21	1
J012147.73+002718.7	1.3947	-0.65±0.02	0.06±0.01	0.48±0.04	4.64±0.01	0.80±0.04	0.93±0.03	1.08	2,3
J085042.21+515911.7	1.3265	-2.70±0.02	0.41±0.01	0.61±0.07	4.54±0.01	1.21±0.06	0.79±0.05	1.14	4
J085244.74+343540.4	1.3095	-2.98±0.02	0.47±0.01	0.47±0.05	4.55±0.01	0.84±0.05	0.88±0.04	1.40	4
J100713.68+285348.4	0.8839	-3.85±0.05	0.65±0.03	6.45±2.38	4.91±0.15	1.78±0.19	5.69±1.49	1.10	5
J145907.19+002401.2	1.3888	-2.17±0.02	0.08±0.01	9.22±0.71	4.56±0.02	2.68±0.07	5.40±0.27	2.19	2,3
J160457.50+220300.5	1.6405	-2.09±0.01	0.28±0.01	0.46±0.03	4.58±0.01	0.93±0.03	0.75±0.03	1.37	6

Note. — Best fitted parameters of Optical/UV extinction curves for SDSS 2175-Å absorbers.

^aRedshift of interested absorber.

^bThese values are fixed during spectrum fitting.

References. — (1) this work; (2) Wang et al. 2004; (3) Jiang et al. 2010; (4) Srianand et al. 2008; (5) Zhou et al. 2010; (6) Noterdaeme et al. 2009